Nonlinear effects on ENSO's period

Fiona Eccles

1 Introduction

El Niño is roughly defined as the warming of the east equatorial water of the Pacific Ocean about every 3 to 6 years and is accompanied by a "Southern Oscillation" signal in the atmosphere, the events together being known as ENSO. In normal, non-El Niño conditions the trade winds blow towards the west across the tropical Pacific. The sea surface temperature (SST) is about 8 °C higher in the west (so there are relatively cool temperatures off South America) with a corresponding slope in the thermocline, it being deeper in the west. During El Niño the trade winds relax in the central and western Pacific leading to a depression of the thermocline in the eastern Pacific, and an elevation of the thermocline in the west.

Despite much study to understand this complex phenomenon the reason for the particular period of the ENSO event, every 3–6 years, is as yet poorly understood. In this study we examined different El Niño periods in a delayed oscillator model, in particular the behaviour of the wave dynamics and nonlinearity, to further advance our understanding of this issue (at least in the model!) We believe the nonlinearity plays a key role in setting the period in the model and it was specifically this role that we hoped to further comprehend.

However, the ENSO period in the model is dependent not only on this nonlinearity but is also a function of the model parameters. In order to separate out purely the effect of the nonlinearity we ran the model in a chaotic regime with *one* set of model parameters. The different periods present in this regime could then be extracted as unstable periodic orbits, using the method outlined below. Thus it was possible to examine various ENSO frequencies with the *same* model parameters and therefore study solely the effect of the nonlinearity on the wave dynamics. It is important to note that the use of the chaotic regime is merely a tool used here. The results regarding the effect of the nonlinearity on the period of ENSO should also be valid when ENSO is in a non-chaotic regime.

This report is structured as follows. In the next section we present the evidence for the four year El Niño cycle and the failure of a current GCM and of linear theory to fully reproduce or explain this. In section 3 there is a brief outline of the model used for this study, and the model's transition to chaos, the state used to examine the role of the nonlinearity, is shown in section 4. The method of finding unstable periodic orbits (UPOs), the cycles with different periods within the chaos, is described in section 5. Section 6 presents an observation of an amplitude-period relationship in the model, found using the UPOs, with a comparison with the Cane and Zebiak [1] model. The wave dynamics analysis of the results is presented in section 7 before concluding remarks (section 8) and acknowledgments.

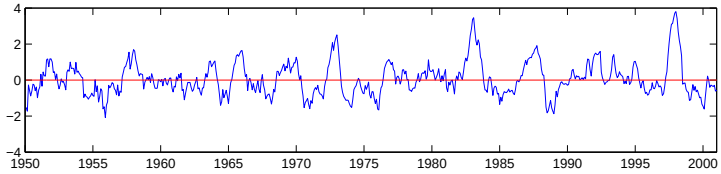

Figure 1: Niño3 record (average SST 5N-5S, 150W-90W) for 1950-2001, data from http://www.cpc.ncep.noaa.gov/data/indices/, figure courtesy of Eli Tziperman.

2 ENSO's period

2.1 The observations

The Niño3 record, figure 1, shows the average SST in an equatorial region of the east Pacific which corresponds to the region where El Niño warming is observed. This clearly shows the ENSO cycle over the last 50 years, with a period of 2–6 years, and indeed a power spectrum of such records yields a broad peak at around four years. However it would appear the El Niño cycle is not just a feature of the Holocene climate (see e.g. Hughen et al. [2]). Information about the temperature in the last interglacial period (120,000 years ago) can be inferred from the exoskeletons of coral. The amount of the heavy isotope ^{18}O absorbed depends on the SST and the quantity of the isotope in the surrounding water (which depends on precipitation and evaporation rates). Cooler SSTs and drought conditions caused during El Niño in Indonesia (from where the coral record was extracted) create large positive anomalies in the ^{18}O record. The evidence here too points to a broad peak around a similar timescale in the power spectrum.

2.2 Models

Simulating and/or explaining this cycle at around four years is proving to be a challenge to the climate community. GCMs often get the period wrong; usually it is too short. For example Timmerman et al. [3] performed runs with a GCM with an increasing greenhouse gas scenario to evaluate the impacts this might have on El Niño. They concluded that this scenario had little effect on the El Niño period (although the same was not true for the amplitude of the event.) However the El Niño period in their control runs is 2 years, i.e. too short by a factor of 2! It would be interesting to be able to explain the period in this model to verify that the result of no change in period didn't depend on the control run period.

2.3 Linear analysis

Münnich et al. [4] compare versions of their iterative map model of ENSO with linear and nonlinear ocean-atmosphere couplings. They find that a linear version of their model can only produce periods up to about two years but demonstrate that when nonlinearity is included periods more akin to the real world ENSO are produced. They postulate that the mechanism choosing the preferred period (of approximately 4 years) is in essence nonlinear.

For our study we used a similar, though simplified, delayed oscillator type model, which is described in the next section. As linearised analysis seems unable to fully explain the

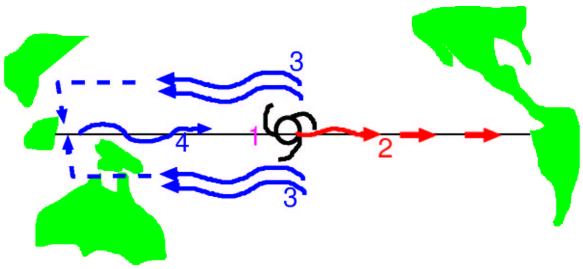

Figure 2: The delayed oscillator mechanism (see text for description), figure courtesy of Eli Tziperman.

source of ENSO's period it was the purpose of this project to explore nonlinear effects on the period in a delayed oscillator model. More specifically we asked the following two questions: what role could nonlinearity play in setting or affecting ENSO's period? Is there a relation between the period of ENSO and its amplitude?

3 The delayed oscillator

The delayed oscillator description of El Niño (Suarez and Schopf [5], Battisti [6]), can be described as follows (see figure 2). An easterly wind weakening (1) creates an equatorial warm (downwelling) Kelvin wave (2) that travels to the east Pacific arriving within 1–2 months, where a thermocline rise induces SST heating and starts an El Niño. The event is amplified by ocean-atmosphere instability: the SST heating causes further wind weakening therefore there is a positive feedback that strengthens the east Pacific warming. However the original wind weakening also creates off-equatorial (upwelling) Rossby waves (3) which propagate westward and are reflected from the western boundary as cold Kelvin waves (4) to arrive six months later at the eastern boundary and terminate the event. The equation which Suarez and Schopf [5] used to capture this behaviour in the SST ($T(t)$) is (in nondimensional form)

$$\frac{dT(t)}{dt} = T(t) - \alpha T(t - \delta_T) - T^3(t)\,. \tag{1}$$

The first term represents the positive feedback effects of the Kelvin wave (ignoring the short delay in the time for it to travel to the eastern basin), the second term is the Rossby wave and the third a nonlinear damping term to stabilise the system. δ_T is the nondimensional Rossby wave delay time and α measures the influence of the returning signal relative to that of the local feedback (i.e. relative to the Kelvin wave term.) This model produces oscillations, although whether or not the timescale of these oscillations is the required 3–6 years depends sensitively on the specific model parameters chosen so ENSO's period is not a robust feature of this model.

We now go on to consider the delayed oscillator used for the present study.

3.1 A brief derivation of the delayed oscillator used here

Models of ENSO when run in certain parameter regimes can generate SST behaviour which is self-sustained and periodic; the period obtained depends on the model parameters. However we wanted to extract the role of nonlinearity on the period separately from the role of parameters and for this it is necessary to run the model in a chaotic regime in a way which shall be outlined in section 4 onwards. First we shall describe briefly the model used though the reader is referred to [7] and the references therein for a full description. The model we used in this study was that of Galanti and Tziperman [7] (hereafter GT). It is based on that of Jin [8, 9] which is turn is simplified from the model of Zebiak and Cane [1], hereafter CZ.

3.2 Ocean dynamics

The ocean dynamics follow from a shallow water anomaly model on an equatorial β plane with linear friction using the long wave approximation, (i.e. no $\partial v/\partial t$ term). The meridional damping and meridional wind stress are also neglected. The resulting set of equations is

$$\begin{aligned} \frac{\partial u}{\partial t} - \beta y v + g' \frac{\partial h}{\partial x} &= \epsilon_m u + \frac{\tau_x}{\rho H}\,, \\ \beta y u + g' \frac{\partial h}{\partial y} &= \epsilon_m v + \frac{\tau_y}{\rho H}\,, \\ \frac{\partial h}{\partial t} + H(\frac{\partial u}{\partial x} + \frac{\partial v}{\partial y}) &= -\epsilon_m h\,, \end{aligned} \tag{2}$$

where u and v are the zonal and meridional anomaly velocities, h is the thermocline depth departure from its mean state, g' is the reduced gravity acceleration, ϵ_m is the oceanic damping coefficient, and H is the mean thermocline depth. Jin makes the "two strip approximation" which assumes that the ocean dynamics in the equatorial region is well represented by a combination of equatorial Kelvin waves and off-equatorial long Rossby waves. The ocean basin is also divided into two zonal boxes. GT instead of using the two box approach integrate along characteristics for Kelvin waves (along the equatorial strip) and Rossby waves (along the off-equatorial strip) to obtain a delay equation. The Kelvin delay time is retained in GT's analysis, and is neglected by Jin.

3.3 The ocean-atmosphere interaction

GT follow Jin in that they have a (truncated) Gill's atmosphere; CZ use a full Gill's atmosphere. The wind stress is assumed to affect the waves only in the central part of the basin and is assumed to be a linear function of SST on the eastern equator (Jin [8]),

$$\tau_x(t) = \mu(t) b_0 T(t) \exp(-\frac{y^2\alpha}{2L_0^2})\,, \tag{3}$$

where $\sqrt{\alpha}/L_o$ is the atmospheric Rossby radius of deformation, b_0 is the annual mean coupling and $\mu(t)$ a seasonally varying coupling. Thus the analysis of GT yields an equation for the thermocline depth anomaly in the eastern equatorial Pacific, h,

Parameter	Description
h	thermocline depth anomaly on the Eastern equator
T	temperature anomaly on the Eastern equator
ϵ_m	oceanic damping coefficient
τ_2	Kelvin wave basin crossing time
τ_1	Rossby wave basin crossing time
r_W, r_E	the reflection coefficients at the western/eastern boundaries
$dt = 0.5$	the fraction of crossing time that wind stress affects waves
ρ	mean density of ocean
A^*	a constant relating wind stress anomalies to SST anomalies
b_0	annual mean coupling strength
μ	relative coupling coefficient which changes seasonally
$\bar{w}$	mean upwelling
ϵ_T	thermal damping coefficient
T_{sub}	temperature anomaly at depth H_1; a function of h
h	thermocline depth anomaly
γ	relates the temperature anomalies entrained into the surface layer to the deeper temperature variations due to $T_{sub}(h)$.

Table 1: Parameters in equations 4 and 7.

$$\begin{aligned} h(t) &= e^{-\epsilon_m \tau_2} r_W r_E h(t - \tau_1 - \tau_2) e^{-\epsilon_m \tau_1} \\ &- e^{-\epsilon_m \tau_2} r_W \frac{1}{\beta \rho} A^* dt \tau_1 \mu(t - \tau_2 - \frac{\tau_1}{2}) b_0 T(t - \tau_2 - \frac{\tau_1}{2}) e^{\epsilon_m \tau_1/2} \\ &+ \frac{1}{\rho C_o} dt \tau_2 \mu(t - \frac{\tau_2}{2}) b_0 T(t - \frac{\tau_2}{2}) e^{\epsilon_m \tau_2/2} \,. \end{aligned} \tag{4}$$

where the model parameters are described in Table 1. Equation 4 can be physically interpreted as the thermocline depth anomaly due to signals propagated by slow moving Rossby waves and faster Kelvin waves. In the GT model the wind stress excites these waves which are responsible for the El Niño event. The seasonal coupling μ is given by

$$\mu = 1 + \delta \cos(w_a t - \phi). \tag{5}$$

$w_a = 2\pi/12$ is the annual frequency and $\phi = 5\pi/6$ is the phase; the coupling peaks in May. This represents the fact that the strength of the response of the wind stress anomalies to SST anomalies varies with season. It has several contributions (see Tziperman et al. [10] and GT), chief amongst them the variation of the mean wind convergence due to the movement of the ITCZ. Another important contribution is the seasonal variation of the mean SST.

All Rossby waves move westward across the basin damped by $e^{-\epsilon_m \tau_1}$, travelling along the off equatorial strip, whereas the Kelvin waves move eastward as damped equatorial waves ($e^{-\epsilon_m \tau_2}$). τ_1 and τ_2 are the basin crossing times for Rossby and Kelvin waves respectively and r_W (r_E) the reflection coefficient at the western (eastern) boundary.

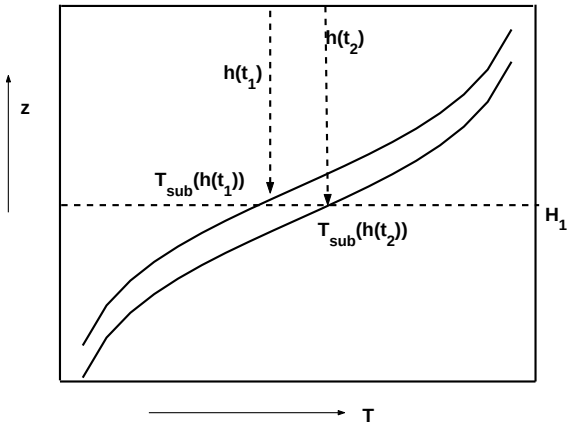

Figure 3: A schematic of the variation of T_{sub} with the movement of h. At t_1 the thermocline is nearer the surface and thus the temperature T_{sub} (measured at depth H_1) is less than when the thermocline is deeper at time t_2.

At each timestep equation 4 has three contributions. The first term on the RHS represents a "free" wave which left the eastern basin (after a reflection by the eastern boundary) at a time $t - \tau_1 - \tau_2$ and travelled as a Rossby wave, to the western boundary arriving at time $t - \tau_2$. It was then reflected by the western boundary and travelled back to the eastern boundary as a Kelvin wave, arriving at time t. The second term represents the Rossby waves excited at a time $t - \tau_2 - \tau_1/2$ in the central Pacific which travelled westward, again being reflected at $t - \tau_2$ and which travelled back as a Kelvin wave arriving again at t. The final term is a Kelvin wave, excited at a time $t - \tau_2/2$ in the centre of the basin which then travelled to the eastern basin. Note the negative sign for the Rossby wave term due to the fact it is proportional to the curl of the wind stress (the Kelvin wave term is proportional to the wind stress itself, hence a positive feedback). Thus a weakening of the westward winds results in an excitation of warm Kelvin waves and cold Rossby waves (and a strengthening of the winds leads to vice versa); hence the system oscillates.

3.4 The SST equation

The model solves equation 4 coupled with an equation for the evolution of SST. GT follow Jin and keep only the time rate of change, the advection by the mean upwelling $\overline{w}$ and the damping term (cooling) from a usual advection diffusion temperature equation.

$$\frac{\partial T}{\partial t} = -\epsilon_T T - w\frac{\partial T}{\partial z} \tag{6}$$

The second term on the RHS is parameterised, following CZ, as

$$\gamma\frac{\overline{w}}{H_1}(T - T_{sub}(h))\,,$$

where T_{sub} is the temperature anomaly at depth H_1 (the mean thermocline depth) and is approximated as a tanh function (Münnich et al. [4]). This is explained in figure 3.

Hence the SST in the east varies as

$$\partial_t T = -\epsilon_T T - \gamma \frac{\bar{w}}{H_1}(T - T_{sub}(h))\,. \tag{7}$$

Note that the main nonlinearity in the model is due to T_{sub} and that the mechanism of oscillation in the GT model has an explicit delay for the time it takes SST to adjust to changes in h.

4 Transition to chaos

As we stated in section 3, in order to separate the role of nonlinearity from that of the parameters in setting the period of El Niño we have used the idea of running the model in a chaotic regime. This will become clear as we proceed below. We changed the parameters b_0 and μ, i.e. the mean coupling and the seasonal coupling in the search for chaos. To diagnose the chaos we examined the time series of temperature, the frequency spectrum and the reconstructed delayed coordinate phase space. The latter of these is found as follows. Take the data set of SST output every day and from this form a subset of the data subsampled every year, $T(t)$. Then plot $T(t)$ versus $T(t-\tau)$ where τ is one year.

The GT model follows the quasi-periodic route to chaos (Tziperman et al. [11]), as opposed to that of period doubling or intermittancy. As b_0 and μ (or equivalently δ) are changed the model exhibits different types of behaviour.

It should be noted that for oscillations to be sustained the coupling must be greater than a critical value otherwise the damping of the waves overcomes the positive feedback effect as described in section 3 and a constant temperature results.

4.1 The quasi-periodic regime

In this regime the ratio of the frequency of El Niño (ω_{el}) to the seasonal cycle (ω_a) cannot be written as a rational fraction i.e. it is not possible to write ω_{el}/ω_a as n/m where n and m are integers. An example with period of approximately 4.35 years can be seen in figure 4. The phase space Poincaré section is a closed loop and the time series is periodic. The spectrum demonstrates there are other frequencies present, due to the nonlinearity of the oscillation.

4.2 The mode locked regime

In this regime the signal is locked to some rational multiple of the seasonal cycle. For this type of chaos we need a damped nonlinear oscillator forced by a period forcing. This regime is seen in figure 5; the frequency for this particular choice of parameters is 1/4 the annual period.

4.3 The chaotic regime

In figure 6 the spectrum shows a very broad peak at around 3-4 years which together with the phase plot identifies this as a strongly chaotic regime and hence the one we shall use for our study.

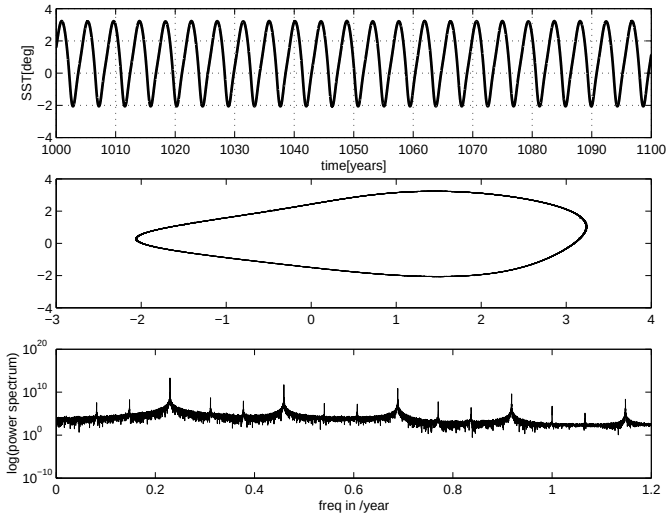

Figure 4: SST for a b_0=7.5×10^{10} kg month^{-2} m^{-1} $^{\circ}C^{-1}$ and δ=0.001

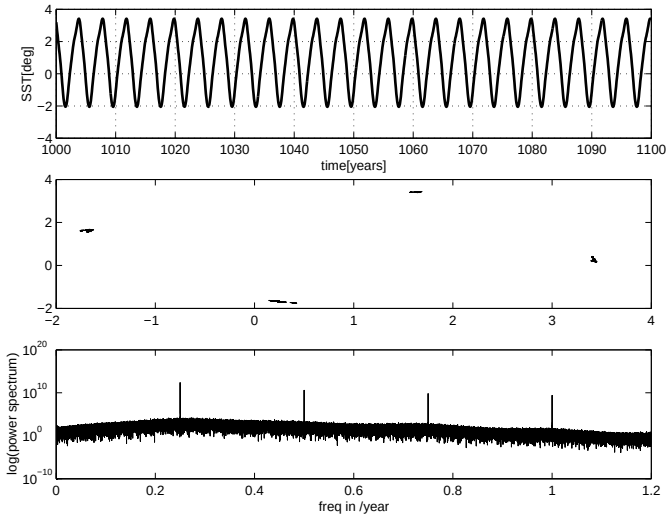

Figure 5: SST for a b_0=7.5×10^{10} kg month^{-2} m^{-1} $^{\circ}C^{-1}$ and δ=0.04

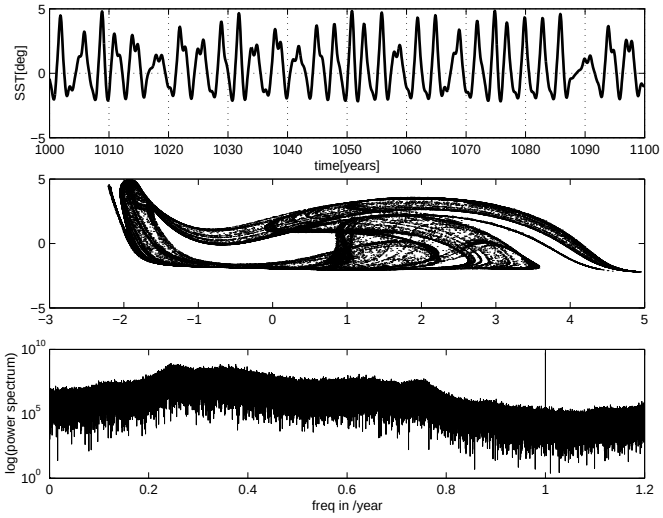

Figure 6: SST for a b_0=7.5×10^{10} kg month^{-2} m^{-1} $^{\circ}C^{-1}$ and δ=0.18.

4.4 Other periods

As an aside we mention as stated in section 2, that the model can support varying periods depending on the model parameters. Figure 7 for example shows an example of a longer period than figure 4 (the period is approximately 9.9 years in contrast to the 4.35 years of figure 4), while still being in the quasi-periodic regime.

5 Finding unstable periodic orbits

We wanted to compare the wave dynamics of several different periods of El Niño which the model supports. As the model is now in the chaotic regime, different periodical solutions exist as unstable periodic orbits; we have many different El Niño periods for the *same* values of the model parameters.

To enable us to study the unstable periodic orbits (UPOs) we ran the model in the chaotic regime for 100,000 years, with output every day to obtain a time series of the SST, T(t). Then following the method outlined in Tziperman et al. [12], we determined the UPOs in a 3 dimensional delay-coordinate phase-space reconstruction from the T(t). The delay coordinates are defined as $\mathbf{X}(t) = \{X_1, X_2, X_3\} = \{T(t-2\tau), T(t-\tau), T(t)\}$ where τ is one year. For a given period p we searched for phase space points $\mathbf{X}(t)$ that returned to the same neighbourhood after a period p, so that $||\mathbf{X}(t) - \mathbf{X}(t-p)|| < \epsilon$ for some small ϵ. When plotting the number of peaks which fall into this criterion against p, the UPOs show up as peaks (figure 8). The points $\mathbf{X}(t)$ which satisfy the above criterion for p= 3,4,5 and 6 years can be seen in figure 9. Note there are two separate three year UPOs and the six year one appears to be just a period doubling of that for three years. It is then necessary to extract one orbit for each of the UPOS, i.e. one "loop of the circuit". We can then also examine the corresponding segment of the time series and subsequently the wave dynamics for each of the segments. The single UPOs are shown in figure 10 with the corresponding

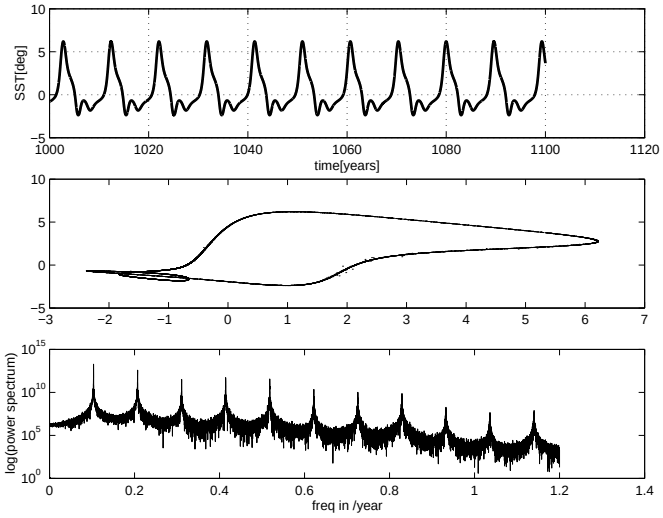

Figure 7: SST for a b_0=8.5×10^{10} kg month^{-2} m^{-1} $^{\circ}C^{-1}$ and δ=0

time series in figure 11.

For our study we wanted to examine the dynamics of "independent orbits". From figure 11 it is evident that the five and eight year orbits are composed of two other UPOs; the five year one being composed of a two year orbit and a three year orbit for instance. The two shorter period UPOs have merged in phase space to form the five and eight year UPOs. In order to build up the wave dynamics picture therefore we concentrated our attention on the three and four year UPOs.

The system jumps irregularly between the different UPOs (not just those pictured). With no seasonal cycle present the "natural" El Niño period is largely about 3–5 years. It would be no surprise therefore if the system spent most time near the three, four and five year UPOs, i.e. they were the least unstable.

6 Amplitude period relations in the delayed oscillator

From figure 12 it is feasible to postulate an amplitude period relationship; the shorter period has a larger amplitude. This seems to be true of even the merged orbit; at least the two year cycle visible in figure 11c (as part of the five year UPO) has a still larger amplitude than either the three or four year SST series. This relationship is not in general true of nonlinear oscillators. For example the unforced Duffing oscillator/spring equation

$$\ddot{x} + \omega^2 x + bx^3 = 0\,,$$

yields solutions for both a spring which increases in frequency ($b > 0$) with increasing amplitude and the converse[1] ($b < 0$). So how robust is our amplitude frequency relationship? Also, what might be the physical mechanism behind this relationship?

[1]The question may well be asked as to whether this is a good comparison to make, after all the spring is an undamped, unforced oscillator, however we mention it briefly as a first thought. A better comparison might be to look at something like the Lorenz equations.

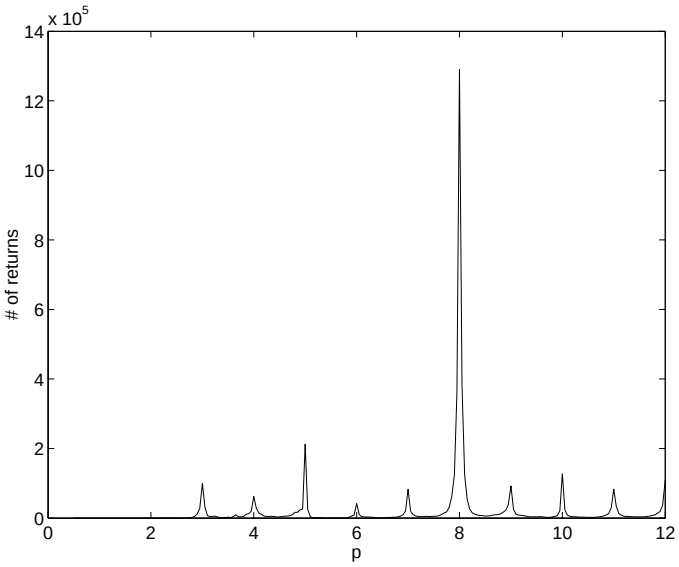

Figure 8: Number of returns for each value of p, ϵ=0.02.

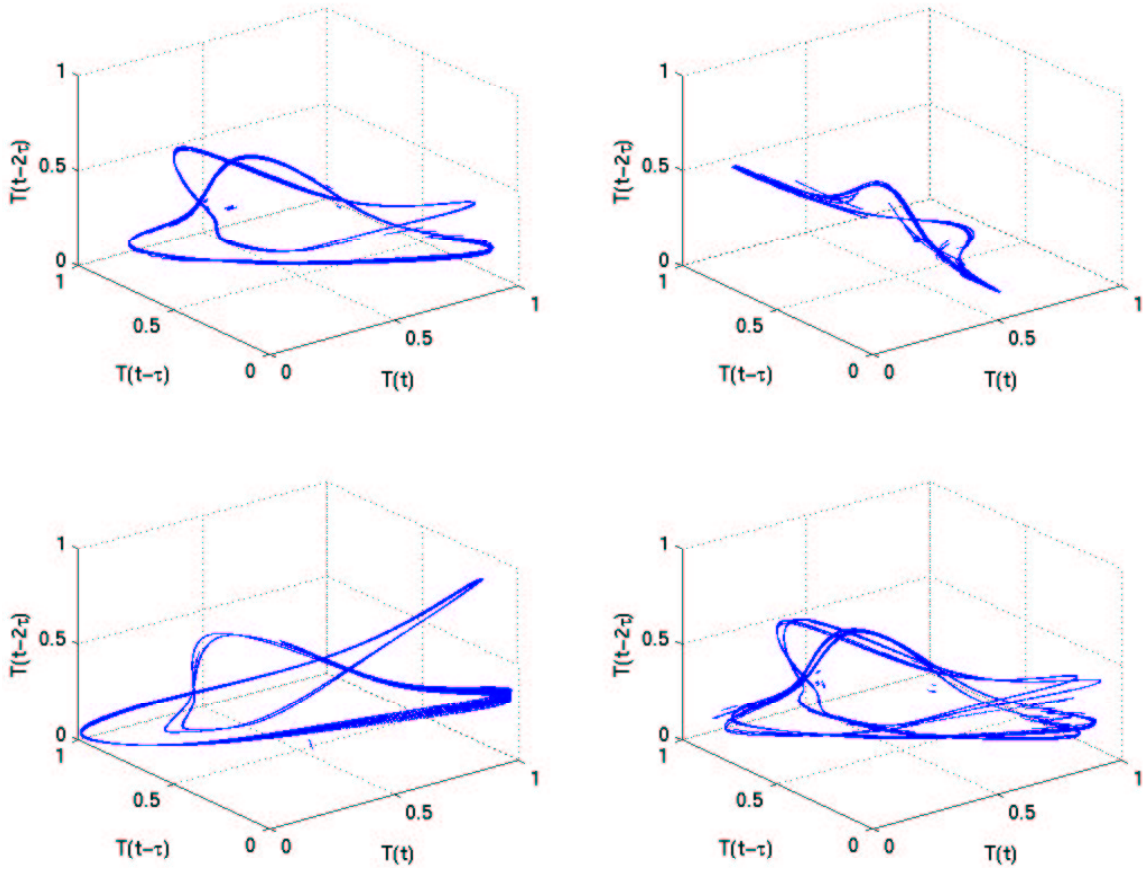

Figure 9: UPOs for a)p=3, b)p=4, c)p=5, d)p=6 years

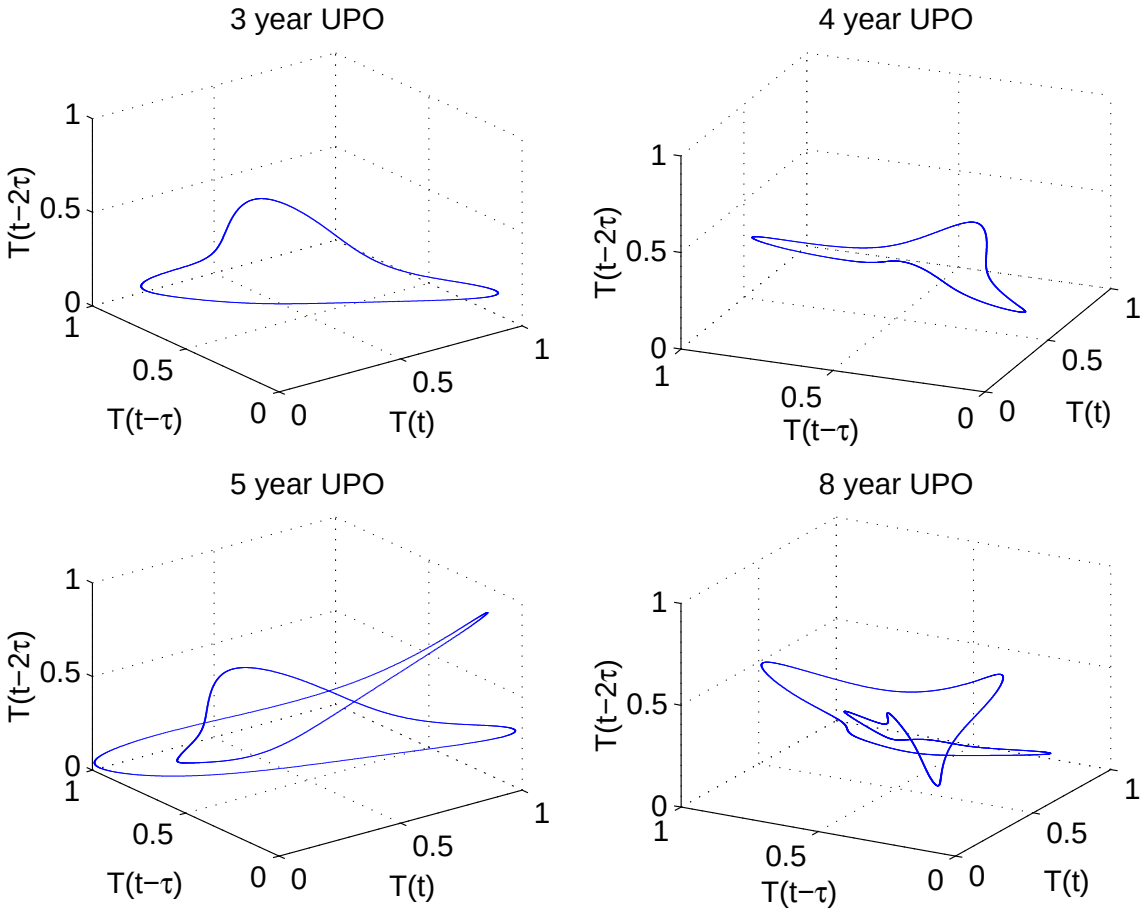

Figure 10: Single UPOs for a)3 years and b)4 years c)5 years and d)8 years

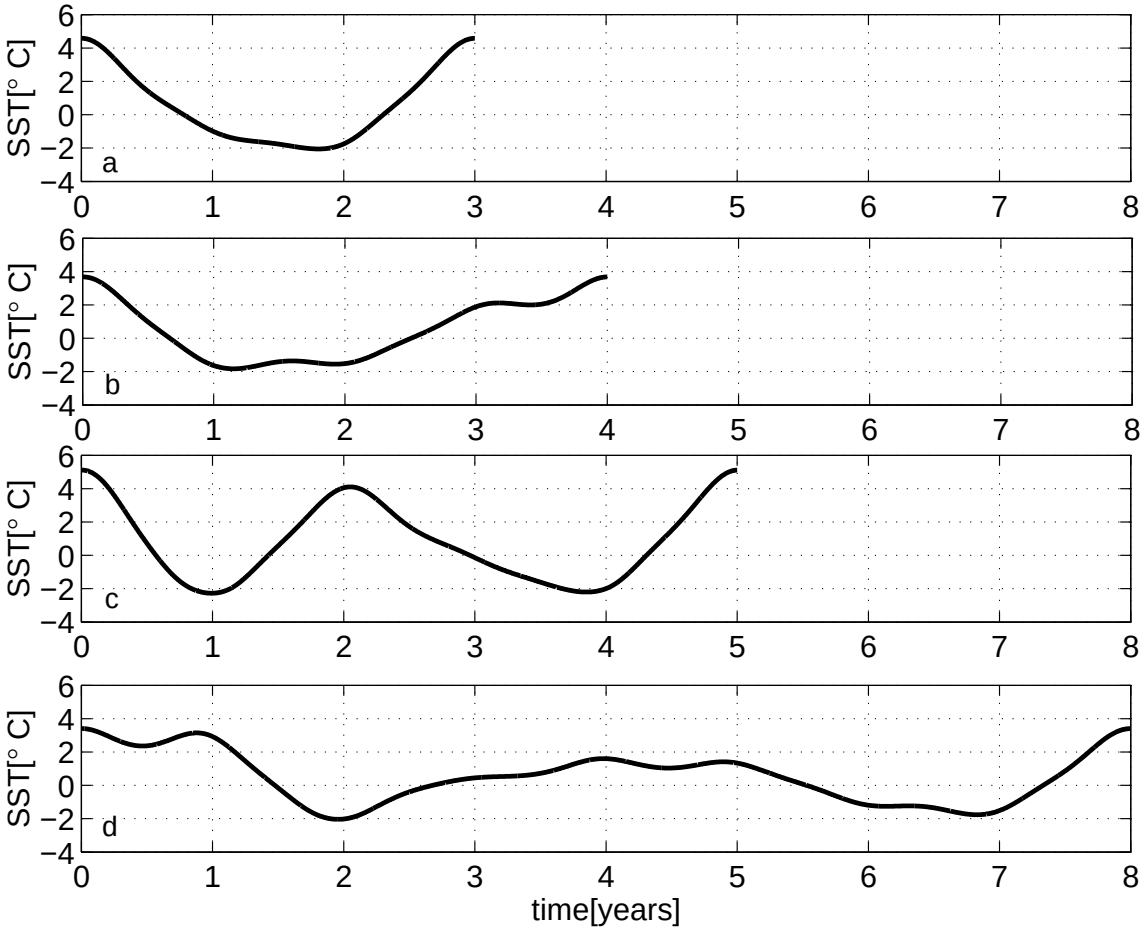

Figure 11: SST for a)3 years and b)4 years c)5 years and d)8 years

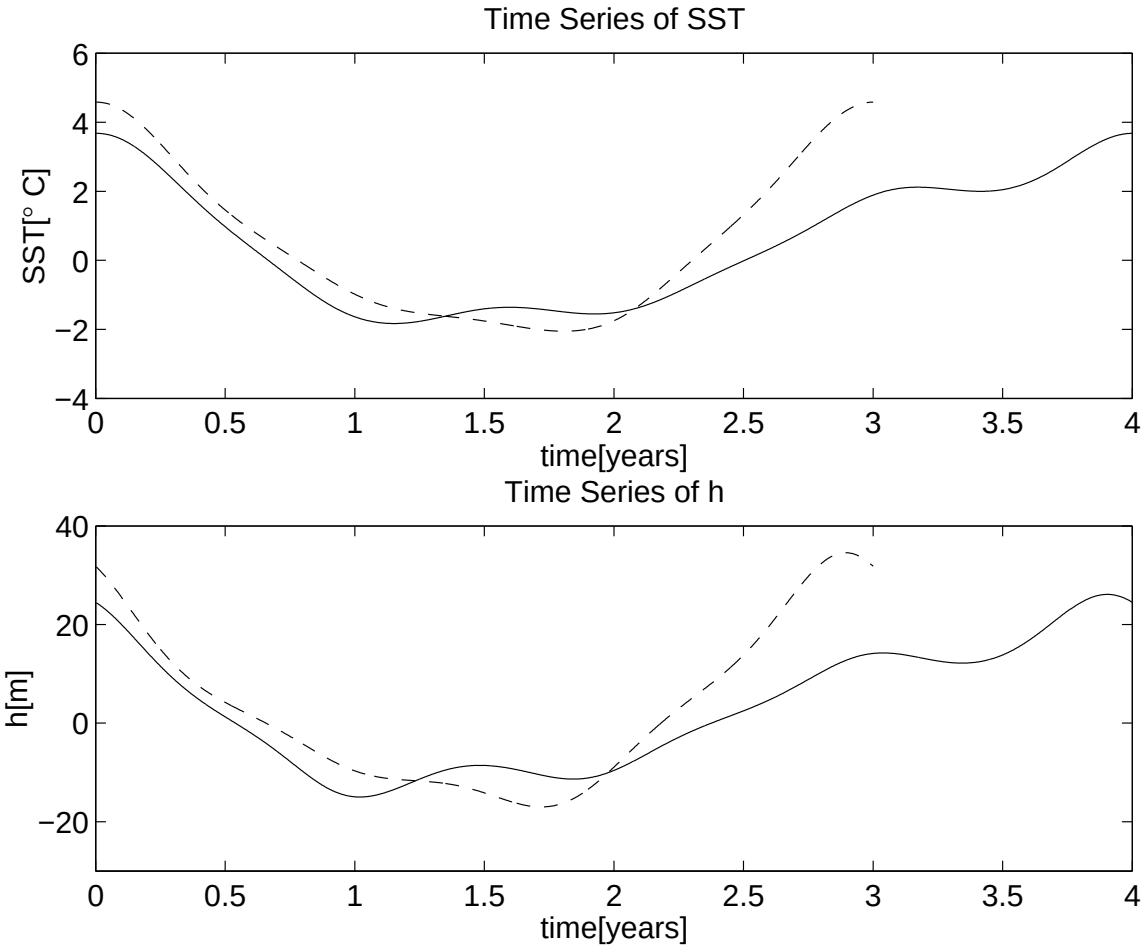

Figure 12: SST and h for the three ($-\ -$) and four (–) year UPOs

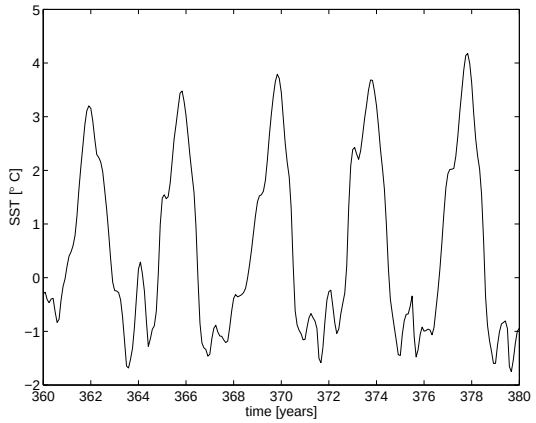

Figure 13: A section of a time series from the Cane-Zebiak [1] model showing events with an amplitude of just over 3°C.

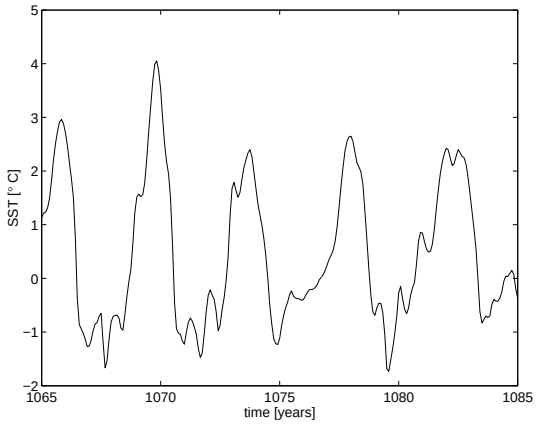

Figure 14: A section of a time series from the Cane-Zebiak [1] model showing events with an amplitude of just over 2 °C.

6.1 The Cane-Zebiak (1987) model

As a quick check on the amplitude frequency relationship we performed a preliminary comparison with the CZ model, mentioned in section 3.1. Looking at examples of El Niño events at just over 3°C (figure 13) and comparing them with those just over 2°C (figure 14) the periods appear to be about the same (4.1 years in the former case and 3.9 years in the latter case.) As a further example in figure 15 the smaller (just over 2°C) and larger events (just over 3°C) both have periods of exactly 4 years.

An examination of events smaller than 2 °C is problematic as it is depends very much then on the definition of an event. By how much does the SST have to warm before an El Niño is said to have taken place? Some of these small events/noise can be seen in figures 13 to 15. This preliminary investigation seems to suggest no clear period amplitude relation in the CZ data, however a fuller statistical analysis is clearly needed.

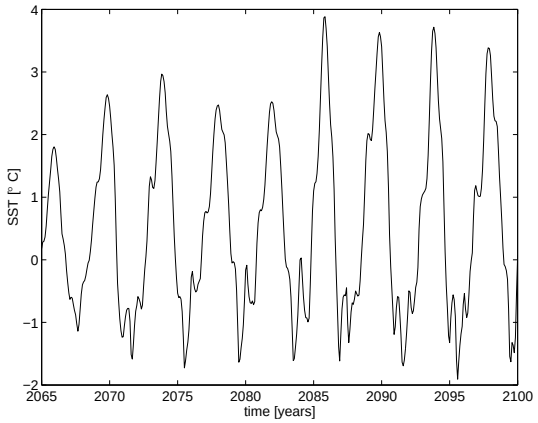

Figure 15: A section of a time series from the Cane-Zebiak [1] model showing consecutive events with amplitudes of just over 2 °C then just over .3 °C.

7 Wave dynamics analysis

Returning to look at figure 12 we can compare the features of the three and four year ENSO cycles. The four year cycle spends time between one and two years at an approximately constant temperature and the four year warming which begins around two years is longer and more gradual. To attempt to explain this behaviour in terms of the waves dynamics we examined the various terms in equation 4, and they are plotted for each UPO in figures 16 and 17. We use the following notation for the terms from equation 4. RK is the free Rossby-Kelvin wave, ER is the excited Rossby wave and EK is the excited Kelvin wave as described in section 3.3.

$$\begin{aligned} RK &\equiv e^{-\epsilon_m \tau_2} r_W r_E h_{eE}(t-\tau_1-\tau_2) e^{-\epsilon_m \tau_1} \\ ER &\equiv -e^{-\epsilon_m \tau_2} r_W \frac{1}{\beta\rho} A^* dt \tau_1 \mu(t-\tau_2-\frac{\tau_1}{2}) \times b_0 T_{eE}(t-\tau_2-\frac{\tau_1}{2}) e^{\epsilon_m \tau_1/2} \\ EK &\equiv +\frac{1}{\rho C_o} dt \tau_2 \mu(t-\frac{\tau_2}{2}) b_0 T_{eE}(t-\frac{\tau_2}{2}) e^{\epsilon_m \tau_2/2}\,. \end{aligned} \tag{8}$$

τ_1 is 8.5 months and τ_2 is 2.1 months. The effect on h at any point in time is therefore determined by the SST one month previously (via term EK) and by the SST about 6 months previously (via term ER). In figures 16 and 17 it can be seen that the Rossby wave term always lags the Kelvin wave term by about 6 months (and its amplitude is smaller and with an opposite sign.) The term RK is a slave to the other two as it only depends on h about 10.5 months before.

7.1 The three year event

Examine first figure 16. From approximately two years the Kelvin wave (EK) feedback produces higher and higher SSTs as we enter an El Niño event as described in section 3. The warmer SSTs however (via the weakening wind) also cause the generation of cold

Rossby waves which terminate the El Niño event at the end of year three. They then continue to bring a cooling signal such that the temperature begins to decrease and then the Kelvin wave feedback causes an increasing cooling of temperature until this is stopped again by the Rossby wave bringing a warming signal once more towards the end of the second year.

The balance between the Rossby and Kelvin waves required to terminate an event can only happen at the end of the year (see GT). Equation 3 for μ parameterises the coupling between atmosphere and ocean as being strongest in month five. i.e. the system is most unstable then. At the end of the year the coupling of the SST (which is generating the Kelvin term) is much weaker. However the Rossby wave signal felt by the east Pacific at the end of the year is due to the coupling 6 months previously, (when the coupling was strong). Thus a strong warming trend due to the Kelvin waves amplified by weak coupled instability balances the weak cooling trend due to Rossby waves amplified by a stronger coupled instability.

7.2 The four year event

For the first year the picture looks similar to the three year case, figure 18. However at about one year the Kelvin wave has a period of approximately constant amplitude; it seems to get "stuck". Hence six months later the Rossby wave has a similar constant period. At the end of year two the Rossby wave is, as in the three year case, strong enough to cause the warming to begin. The Kelvin wave feedback ensures continuing warming. However as the Rossby wave was constant for a year, by the end of year three it isn't "powerful enough" (i.e. it isn't cooling strongly enough) to cause a halt to the warming. The SST perturbation it was coupled to six months previously was around zero (see figure 12). Hence the Kelvin wave feedback continues to cause warming. As we progress in the third year the Rossby wave becomes stronger and hence limits the amount of warming caused by the Kelvin wave, thus the El Niño amplitude is smaller and finally at the end of year four the event is terminated.

The key then, to the four year cycle developing as opposed to a three year event is the halt of the cooling of the Kelvin wave at the end of the first year. The reason for this presumably involves the nonlinearity but a precise explanation is not immediately apparent. What we can say is that the four year event being weaker is consistent with the fact that the Kelvin and Rossby waves are weaker. This weakness makes the event develop more slowly, and in particular shift from phase to phase more slowly as described above. The stronger three year event sustains stronger Kelvin and Rossby terms which are able to shift the system from El Niño to La Niña faster. This wave dynamics perspective into the amplitude-period relation for the delayed oscillator model used here gives us some intuition regarding the physical processes responsible for this relation.

8 Concluding remarks

The mechanism causing ENSO's robust four year period is not yet fully understood and when simulated in models the explanation seems to rely on a nonlinear effect. In order to separate the nonlinear causes from those of the parameters we extracted UPOs from a

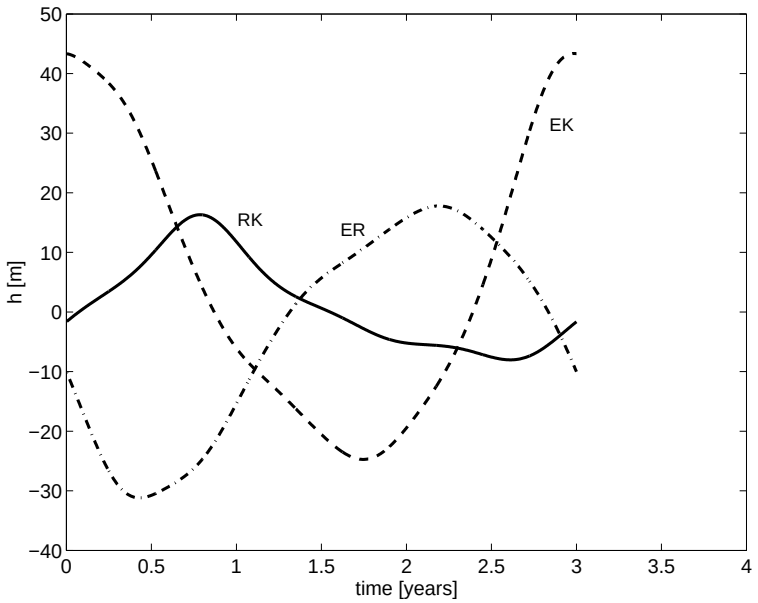

Figure 16: Terms in equation 4: RK(–), ER(−·), EK (− −)

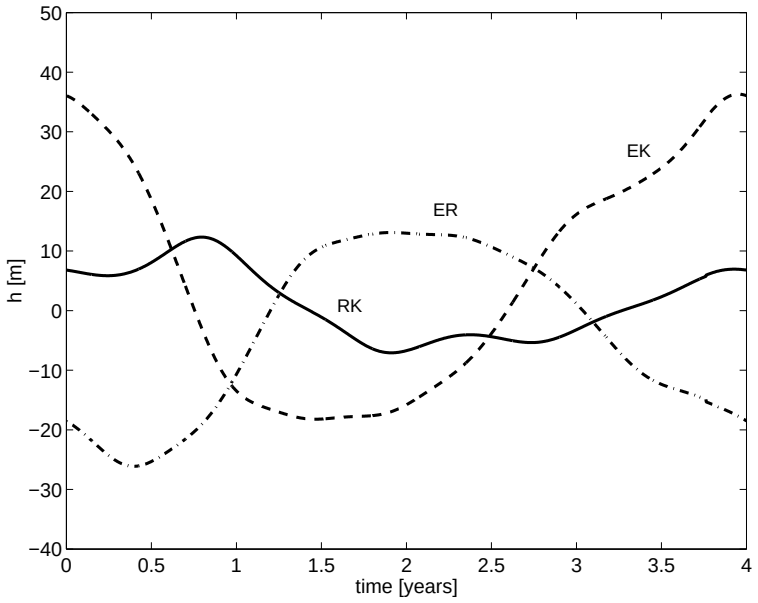

Figure 17: Terms in equation 4: RK(–), ER(−·), EK (− −)

simple delayed oscillator model. We found from these UPOs that a shorter period implied a larger amplitude of an El Niño event and whilst the precise nature of the nonlinearity was unclear it was possible to rationalise this amplitude period relation in terms of equatorial wave dynamics. Efforts to verify this relation with the CZ model were inconclusive at this stage. Further work is required to test its robustness in both fuller models and in the actual Pacific.

9 Acknowledgments

Many thanks indeed to my supervisor Eli Tziperman for suggesting the project and for his patience and guidance in teaching me so much in such a short space of time. Thanks too to Eli Galanti, for his code, his suggestions and his understanding when I used all the disk space! Thanks to Joe Keller, Bill Young and Lenny Smith for suggestions of ways to think and to my "fellow fellows", for going through it and being there with me. To everyone at Walsh cottage thanks for a great summer!

References

[1] S. E. Zebiak and M. A. Cane, "A model El Niño-Southern Oscillation," Mon. Wea. Rev. **115**, 2262 (1987).

[2] K. Hughen, D. Schrag, S. Jacobsen, and W. Hantoro, "El Niño during the last interglacial period recorded by a fossil coral from indonesia," Geophys. Res. Lett. **26**, 3129 (1999).

[3] A. Timmerman, J. Oberhuber, A. Bacher, M. Esch, M. Latif, and E. Roeckner, "Increased El Niño frequency in a climate model forced by future greenhouse warming," Nature **398**, 694 (1999).

[4] M. Munnich, M. Cane, and S. Zebiak, "A study of self-excited oscillations of the tropical ocean-atmosphere system. Part II: Nonlinear cases," J. Atmos. Sci. **48**, 1238 (1991).

[5] M. Suarez and P. Schopf, "A delayed action oscillator for ENSO," J. Atmos. Sci. **45**, 3283 (1988).

[6] D. Battisti, "The dynamics and thermodynamics of a warming event in a coupled tropical atmopshere-ocean model," J. Atmos. Sci. **45**, 2889 (1988).

[7] E. Galanti and E. Tziperman, "ENSO's phase locking to the seasonal cycle in the fast-SST, fast-wave, and mixed mode regimes," J. Atmos. Sci. **57**, 2936 (2000).

[8] F.-F. Jin, "An equatorial ocean recharge paradigm for ENSO. Part I: Conceptual model," J. Atmos. Sci. **54**, 811 (1997).

[9] F.-F. Jin, "An equatorial ocean recharge paradigm for ENSO. Part II: A stripped-down model," J. Atmos. Sci. **54**, 830 (1997).

[10] E. Tziperman, S. E. Zebiak, and M. A. Cane, "Mechanisms of seasonal-ENSO interaction," J. Atmos. Sci. **54**, 61 (1997).

[11] E. Tziperman, L. Stone, M. Cane, and H. Jarosh, "El Niño chaos: overlapping of resonances between the seasonal cycle and the Pacific ocean-atmosphere oscillator," Science **264**, 72 (1994).

[12] E. Tziperman, H. Scher, S. E. Zebiak, and M. A. Cane, "Controlling spatiotemporal chaos in a realistic El Niño prediction model," Phys. Rev. Lett. **79**, 1034 (1997).